# Curved Synthetic Aperture Radar for Near-Field Terahertz Imaging

Mavis Gezimati and Ghanshyam Singh

***Abstract*—High resolution imaging techniques will play an essential role in the future smart imaging applications to provide potential solutions for accurate detection, monitoring and classification of the target. The potential of synthetic aperture radar (SAR) systems to acquire high resolution images has opened new frontiers and led to its exploration in new applications. The conventional microwave radar imaging suffers limited range resolution in the sub-millimeter wave range and optical imaging methods are constrained by the diffraction limit. In the terahertz (THz) regime of the spectrum, the SAR systems could be operated in all the weather, all the time and are capable of penetrating through clouds, smoke, dust etc. to achieve high resolution images beyond the diffraction limit. The curved SAR presents a SAR system created by circularly encircling the target scene. The Circular SAR and Spiral SAR which are based on a circular and cylindrical spiral scanning trajectory, respectively are the scanning methods used for curved SAR. In this paper, we have explored a new toolbox that enables the rapid development of near-field THz-SAR imaging systems and generation of large near-field THz imaging scenarios with the goal to support and facilitate data driven research such as deep learning in the THz community through synthetically generated SAR images as well as its potential for THz based high resolution and 2D/3D near-field imaging application. Initially, the potential advantages of THz-SAR over Microwave SAR and optical imaging methods are presented. Further, a frequency modulated continuous wave (FMCW) radar testbed is simulated in multi-input multi-output (MIMO) configuration for the target frequency band. Moreover, the circular and cylindrical SAR scanning methods are explored for near-field imaging of point targets to obtain 2D and 3D THz-SAR images, respectively. Also, the radar images are reconstructed using the Back Propagation and Polar Formatting Algorithms, focusing on short range applications like indoor environments. Finally, the SAR performance evaluation metrics are reported and a roadmap for future work is presented.**

***Index Terms*—Synthetic aperture radar (SAR), THz imaging, circular SAR, cylindrical SAR, 2D and 3D imaging, near-field, radar image reconstruction, high resolution imaging, reconstruction algorithms, MIMO, FMCW.**

## I. Introduction

ADVANCED imaging techniques for indoor environment monitoring is a very important concept for future generation smart and connected healthcare (healthcare 4.0) monitoring, which require high resolution imaging abilities for accurate localization, monitoring and classification. Lidar and cameras based on near-infrared and visible light facilities are being intensively investigated [1], however their reliance on the optics, limits their performance in bad weather conditions such as snow, rain and fog. Further, the positioning systems at radio frequencies have limited functionality caused by long wavelengths, likewise millimetre wave radars are constrained by restricted range resolution in the sub-millimetre (sub-mm) wave range. Consequently, the ability for all weather sensing and high-performance imaging is anticipated for the future smart indoor monitoring systems, with capability to provide accurate detection through high resolution imaging.

Recently, the higher frequency and short wavelength spectra – the Terahertz (THz) spectrum (0.1 to 10 THz and 30 $\mu$m to 3 mm) has been explored which exhibit great application potential. The potential of sub-mm resolution in the THz regime of the spectrum is attributed to the smaller wavelength and large bandwidth in this frequency region which is located in the transitional band between the macroscopic electronics to micro-photonics [2]. The radar imagers systems based on THz technology are rapidly developing and will be excellent future candidates for fine resolution and all-weather applications [3], [4], [5], [6].

The THz imaging systems are broadly categorized as far-field THz imaging and near-field THz imaging as presented in Fig. 1. The THz imaging categories scope that has been explored in this paper are indicated with yellow colour in the diagram. Both the far-field and near-field THz imaging have been widely explored in various applications as reported in [7]. However, the major limitation of far-field THz imaging is the diffraction limit which affects image spatial resolution. To overcome this challenge, it has been suggested to collect THz signals in the near-field, thus breaking the diffraction limit and provide high spatial resolution [7]. The THz near-field is also classified as: 1) aperture type near-field and 2) aperture-less type near-field [8]. In the aperture type imaging, coherent measurements are implemented on an aperture and the object is focused by propagating the wave backwards to its exact location [1]. The aperture-less type THz imaging uses focal plane imaging whereby the intensity distribution on an imaging plane is measured to illustrate an object. Here, we study the THz aperture type near-field imaging based on Synthetic Aperture Radar (SAR) imaging. The SAR imaging systems utilize the measured THz amplitude and phase from multiple beam paths or multiple positions to reconstruct an image.

Manuscript received 14 February 2023; revised 18 March 2023; accepted 31 March 2023. Date of publication 5 April 2023; date of current version 14 April 2023. *(Corresponding author: Ghanshyam Singh.)*

The authors are with the Department of Electrical and Electronic Engineering Science, Centre for Smart Information and Communication Systems, University of Johannesburg, Johannesburg 2006, South Africa (e-mail: mgezimati@gmail.com; ghanshyams@uj.ac.za).

Digital Object Identifier 10.1109/JPHOT.2023.3264747

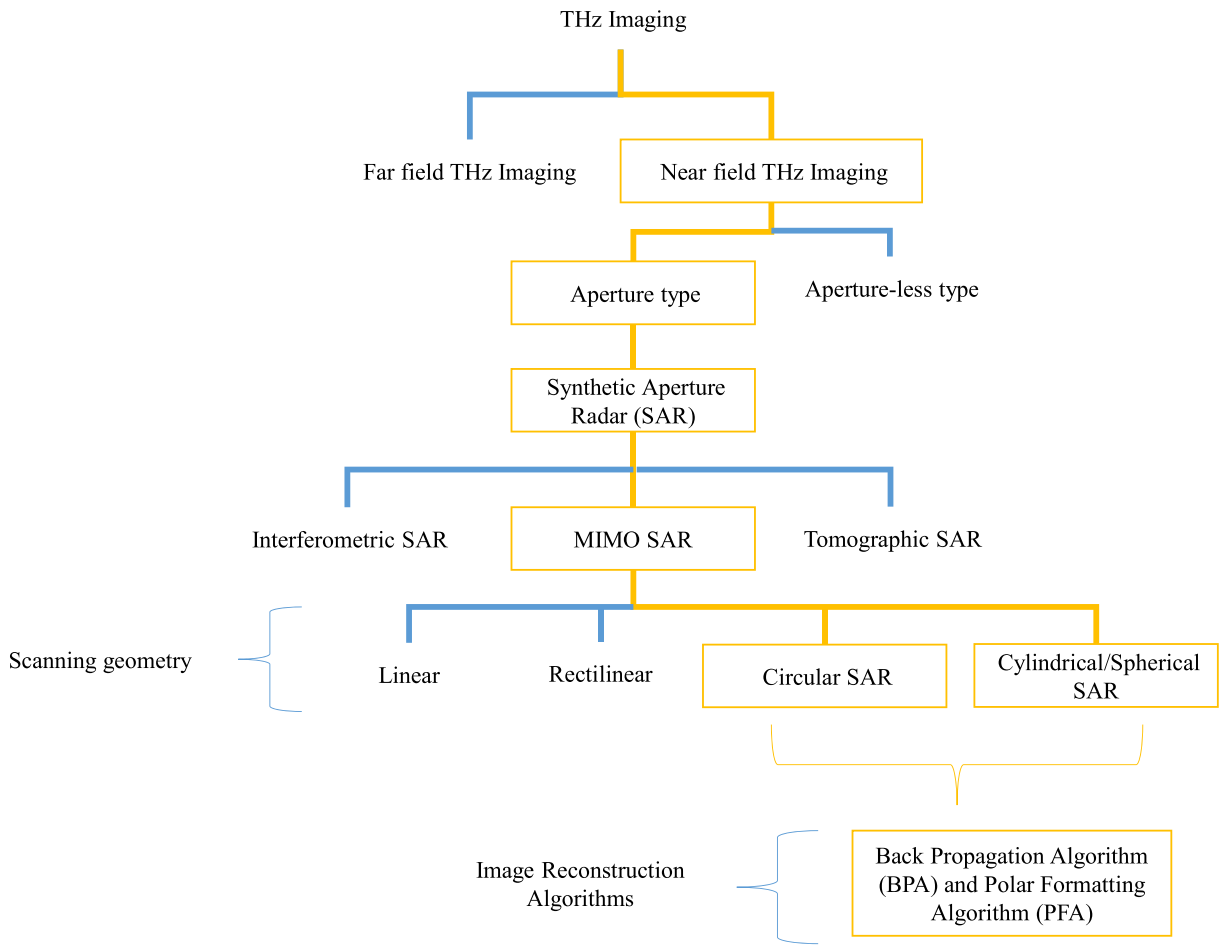


Fig. 1. THz imaging scope explored in this paper.

The SAR imaging based on remote sensing has been broadly applied in the microwave regime of the spectrum (below 30 GHz) and offer a long exploration range. The applications of SAR are being broadened through the THz spectra to high resolution imaging, high resolution localization, material characterization, non-destructive testing (NDT) and near-field imaging and sensing applications. Even though the THz spectrum is limited by sensing range caused by free space path loss and high atmospheric attenuation, however it exhibits great potential to enable imaging applications in the short range or near-field, especially in the indoor environments which could be the basis of more applications for example, household robotics, health monitoring, building fire detection, etc. [7], [9], [10].

Recently, the THz imaging technology has demonstrated salient potential and has become a research hotspot in various applications spanning NDT, radar communication, personal screening, automotive, material characterization, security, object detection and healthcare monitoring. Moreover, its unique characteristics including non-ionizing, non-invasive, high sensitivity to polar molecules such as water and penetrability to dielectric materials play a crucial role in these applications [11]. As a result, the THz based imaging promises great potential as a versatile imaging tool complementary to Magnetic Resonance Imaging (MRI) and X-Ray imaging tools [12]. With the technological advances in THz range, there is a high renewed interest in high resolution and 3D imaging that exceeds the limitations caused by optical sub-elements or illuminating beam through THz imagers based on SAR technique [13], [14].

There are two types of spatial resolution in high resolution imaging for THz systems: 1) range or depth resolution which is not diffraction limited, this depends on pulse spectral bandwidth and not changed by SAR imaging and 2) azimuth resolution which is 2-dimensional and is limited by Rayleigh scattering criterion i.e., the use of optical wavelength. As compared to the microwaves, THz waves provide more spatial resolution, however the conventional THz imaging systems are associated with long scans due to raster scanning whereby pixel by pixel scanning is performed [15], [16]. The SAR system is called curved SAR when the synthetic aperture is produced or created by circularly encircling the scene to be imaged. The circular-SAR (C-SAR) and spiral-SAR (S-SAR) which is based on a cylindrical spiral trajectory are the scanning methods for curved SAR. The C-SAR and S-SAR imaging allow faster scanning with improved resolution and capability of signal-to-noise ratio (SNR) improvement through collecting data measurements from a diverse angular range along full-flight rotation path of 360°

thus accumulating more information of the target scene relative to the linear-SAR (L-SAR) imaging.

### A. Advantages of THz-SAR Over Microwave SAR and Optical Imaging Methods

The THz-SAR is capable of penetrating through dust, smoke, cloud, all weather, day and night, leading to increased target recognition and high-resolution imaging. As compared to the microwave SAR, the advantages of THz-SAR include larger bandwidth, shorter wavelength, higher resolution, higher carrier frequency, aperture speed, frame rate and could be used for real-time imaging and moving target detection at high range resolution [17]. Therefore, it is meaningful to study imaging in the THz regime of the spectrum. As compared to the conventional THz imaging systems based on optics, THz-SAR has potential to achieve better resolution, constant resolution that does not depend on depth of focus linked to optics and better signal-to-noise ratio (SNR) as well as increased acquisition speed. It utilizes radar motion to synthesize a large aperture to yield high angular resolution [18], [19], [20].

The advantages and characteristics of S-SAR and C-SAR include: improved target recognition accuracy through ability to acquire target scattering characteristics in all the directions, high resolution through broadening of effective bandwidth in wavenumber domain and ability to acquire 3D target location information unlike in conventional linear SAR which is limited to 2D [21]. The capability of 360-degree observation of curved SAR makes it more attractive to reconstruct a moving object trajectory or scene.

### B. Related Work

The developments in system-on-chip complementary metal oxide semiconductor (CMOS) radio frequency integrated circuits (RFIC) have resulted in the emergence of cost-effective frequency modulated continuous wave (FMCW) millimetre wave radars for imaging applications. The radar imaging systems include multiple input multiple output SAR (MIMO SAR), interferometric SAR (InSAR) and tomographic SAR [22], [23], [24], [25], [26]. In [8], a THz near-field imaging system based on SAR has been developed for precise, high resolution NDT of packaged aluminium etched antenna arrays and for flexible gold electrode array surface imaging. Novel THz-SAR test-beds based on FMCW radar front-end and vector network analyser (VNA) are being investigated for short range applications including NDT, security/defence, material characterization and automotive [27].

Significant progress has been made on Multi-Input Multi Output (MIMO) multi-static array SAR, with algorithms for 2D and 3D MIMO circular SAR imaging and the SAR imaging technology having been broadly investigated in the microwave spectrum for various applications [28]. In [29], C-SAR technique was applied to develop low cost and compact single channel FMCW radar for a high resolution microwave imaging system. They developed an image reconstruction algorithm and analytically analysed the developed system with discussions of the differences between their system and previously reported systems.

The application of ultra-wideband (UWB) radars in microwave imaging for investigating early and accurate tumour detection has recently gained popularity in breast cancer studies, with image contrast attributed to the conductivity and dielectric permittivity differences between healthy and tumour tissue. The UWB CSAR was explored for breast imaging and for detection of breast tumour based on microwave imaging in [30]. The time domain global back propagation reconstruction algorithm was adapted to circular trajectory acquisition of the data. They also proposed a sectional method for image reconstruction that compensates changes in global velocity for multilayer mediums. The suitability of the system for imaging of breast tumour was examined using experiments on breast phantom designed to emulate normal and tumour tissues through 3D printing fabrication and MRI. When compared to the MRI imaging, the UWB C-SAR demonstrated potential as a tool for early diagnosis and treatment monitoring. The microwave based UWB SAR have also been reported to be suitable for imaging sensing applications in monitoring oil reservoir, wall imaging, material characterization, geo mapping, weather forecasting and tissue imaging [31]. The application of radar based microwave imaging for breast cancer detection has been also investigated in [32] where the matching pursuit algorithm (MPA) has been applied to reconstruct scattering map of the breast from the monostatic Inverse Synthetic Aperture Radar (ISAR) imaging.

The exploration of reconstruction algorithms has been reported in a couple of THz-SAR studies: the inverse Fast Fourier transform was found to reduce computational expenses with more precise ability to focus relative to the back propagation algorithm (BPA) for near-field MIMO-SAR in [33]. While the extended Phase Shift Migration (PSM) was proposed to be more flexible for THz MIMO SAR [34] and the range migration algorithm (RMA) and back propagation algorithm (BPA) were reported to generate different image reconstruction results in THz based SAR, contrary to microwave SAR systems [1]. In [35], an adaptive sub-aperture integration technique for wide angle SAR in THz applications was proposed for improved imaging and [27], 3D SAR was demonstrated at 1.5THz for enhanced image quality relative to the 0.85THz -1.1THz frequency band. Spiral SAR was explored in [2] and a UWB THz FMCW generation technique and UWB signal fusion algorithm was proposed for high range resolution and suitable for multilayer systems [11].

The real time THz SAR was proposed that uses linear motion for imaging in the near field range [36]. A motion error model was proposed for THz CSAR to analyse THz image quality [37]. The potential of fine resolution imaging using a fully integrated FMCW THz-SAR or ISAR was demonstrated by the system developed in [38] which was capable of detecting a plastic ring and a metallic blade. The potential to detect tumour beneath the skin, explosives and moisture level detection as well as contrasting between fat and muscle was demonstrated. The PSM algorithm has been considered better than the BPA, Range Doppler algorithm (RDA) and the RMA was found to reconstruct images with improved precision. The THz based C-SAR

TABLE I
RECENT 3D IMAGING BASED ON THZ SAR

| Reference | THz SAR test bed | Method | Result |
|---|---|---|---|
| [41] | FMCW with frequency range 340GHz to 500GHz. | • All electronic THz 3D sub mm imaging.<br>• High resolution cross range imaging using focused method. | • Good imaging resolution and testing efficiency. |
| [42] | FMCW | • Integration of FMCW and Augmented reality (AR) for a handheld portable THz sensor. | • The feasibility of AR-THz using FMCW was proved.<br>• Simple handling during acquisition.<br>• 3D live superimposed AR view. |
| [43] | FMCW | • Integration of FMCW, line scanning optics and position encoder.<br>• Hand guided THz scanner for NDT. | • The platform demonstrated frequency adaptable. |
| [44] | De-ramped FMCW | • Ray based 2D modelling.<br>• Commercial 3D Finite Difference Time Domain (FDTD) simulator. | • Reduced computation time.<br>• Efficient for sub glacial ice structure investigations. |
| [45] | Not specified | • Estimation of radar cross section of a tree.<br>• Numerical simulations. | • Suitable 3D models were proposed.<br>• Branches have a significant scattering impact which cannot be avoided. |
| [46] | | • THz ray tracing simulations for indoor human posture recording. | • The interaction between human and technical equipment was simulated. |
| [47] | High speed FMCW | • Photonics based approach. | • Up-to 1.3mm spatial and range resolution. |

has been broadly studied in microwave regime of the spectrum, however THz based C-SAR is not yet fully explored. Some of the reported applications for THz radar in short and medium ranges include automotive [35], body security, concealed object detection and indoor localization of people and objects etc. [39]. THz stepped frequency SAR was also explored using an efficient frequency scaling based algorithm that was suggested to perform better than the BPA [40].

There is an increasing interest in THz imaging with 3D imaging capability. Table I presents some of the studies that have recently investigated 3D radar-based imaging at THz frequencies. The capabilities of radar based 3D imaging and sensing has also been recently investigated for various applications including topographic mapping [48], deep learning based approach for moving object localization [49], indoor human vital signs and gesture/activity/posture localization, monitoring and classification [50], [51] and other applications in the THz, radio and microwave frequencies [52], [53], [54], [55], [56], [57], [58], [59], [60]. The capability of SAR technology to achieve 3D imaging and the exploration of efficient reconstruction algorithms in THz and Microwave frequency bands have been reported in various studies including [40], [61], [62], [63], [64], [65].

### C. Motivation

The SAR imaging has been broadly investigated in several microwave applications and generally known to provide high resolution images, however, very limited reported research exists on THz radiation-based SAR. Moreover, only a few studies have investigated on circular SAR and 3D imaging for THz. The conventional THz imaging systems are still very limited by insufficient development status and its high range resolution is usually achieved by a femtosecond THz pulse sources while the azimuth resolution is achieved by electronically or mechanically scanning the target objects using a lens focused beam such as in THz time domain spectroscopy (THz-TDS). Diffraction limit poses a great problem in limiting the spatial resolution which can be resolved using SAR systems.

Therefore, in this paper, we explore the potential of THz radiation-based SAR for near-field imaging applications like indoor environments and note the performance of two reconstruction algorithms based on C-SAR. One of the emerging technologies being used to achieve high resolution imaging is the SAR imaging, which is an active coherent imaging system that supports all weather and all day/night penetration capabilities as compared to that of the optical technology. Additionally, high resolution images enable simplified object localization, classification and identification [9].

### D. Contribution

The paper explores FMCW THz MIMO SAR imaging as a technique for improved spatial resolution and scanning time improvement relative to optical technology and improved spatial resolution as compared to microwave radar imaging. The CSAR imaging is also investigated as a better technique compared to linear and rectilinear SAR. To be more specific:

- We explore a new toolbox that enables the rapid development of near-field THz-SAR imaging systems and generation of large near-field THz imaging scenarios that can be used for data driven applications as well as its potential for THz based high resolution and 2D/3D imaging.
- The advantages of THz based SAR over Microwave SAR and optical imaging methods are reported. Further, the back propagation algorithm (BPA) and polar format algorithm (PFA) based reconstruction algorithms have been explored.
- We will explain the 2D-and 3D-SAR imaging signal processing. Further, an FMCW testbed is simulated in MIMO configuration for the target frequency band.
- We simulate image reconstruction and near-field THz imaging based on C-SAR scanning. Further, we explore a SAR simulator based on THz for near-field applications and comparison of the reconstruction algorithms based on C-SAR is conducted.
- We report evaluation metrics used for SAR performance.

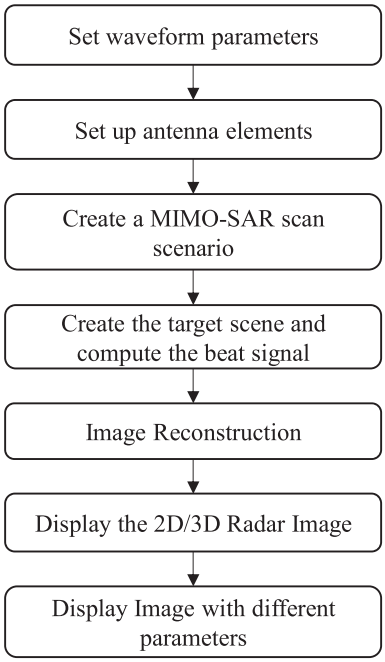


Fig. 2. Flowchart of the THz MIMO-SAR image reconstruction.

### E. Organization

The rest of the paper is organized as follows. The second section describes the materials and methods used and we discuss the attained results in the third section. Lastly, we summarize the paper in the fourth section.

## II. Materials and Methods

The Terahertz Toolbox for simulating near-field THz imaging radar systems [66] are explored. It enables near field THz imaging scenarios generation which could be utilized for various data driven applications. Using a set of programs and Matlab functions, we simulated THz SAR Imaging and radar image reconstruction techniques and algorithms. Fig. 2 shows the flow chat that depicts the THz based SAR imaging and image reconstruction.

### A. THz Waveform Parameters

The first stage involves computing the chirp parameters of THz sensors being tested. The chirp parameters include the FMCW chirp starting frequency, IF (intermediate frequency) signal sampling frequency, device center frequency and total system bandwidth.

The parameters are then used to compute using the following equations:

$$Chirp\ Slope\ K\ = \frac{f_s B}{N_k - 1} \tag{1}$$

where $f_s$ is the IF signal's sampling frequency, $N_k$ is sample wavenumber and $B$ is the bandwidth in Hz. The wavelength $\lambda = \frac{c}{f_c}$, where $c$ and $f_c$ are the speed of light and device center frequency in Hz respectively.

$$Maximum\ Range\ R_{Max}\ = \frac{f_s c}{2K} \tag{2}$$

where $K$ is the Chirp slope in Hz/s.

$$Range\ Resolution\ R_{Resolution}\ = \frac{c}{B_{useful}} \tag{3}$$

where the $B_{useful}$ denote the used bandwidth of the total bandwidth available. The instantaneous frequency ($f$) and instantaneous wavenumber ($k\ =\ (2\pi f/c)$) are then computed using eq. (4):

$$f\ = f_0\ + K\,(t + \tau_{ADC}) \tag{4}$$

where $f_0$, and $\tau_{ADC}$ are the FMCW chirp starting frequency and time constant delay, respectively.

### B. Setting the Antenna Elements/ Array Properties

The physical transmitter (Tx) and receiver (Rx) antenna elements of the radar are set up by specifying the elements' exact location as well as adding, enable or disable individual elements. To compute the *x*-coordinate of each element, values of $x(\lambda) + x(mm)$ are added where $x(\lambda)$ and $x(mm)$ are the number of wavelengths and millimeters, respectively. In this way, the antenna element locations are entered as fractional multiples of the wavelength (which is common), with added offsets in millimeters. In the same way, the $y$ coordinate is calculated. The generation of the MIMO array is in the form of a planar array that is located at the $z$ coordinates specified by the "Transmitter Z(m)" field which automatically updates the "Receiver Z(m)" to match the changes of field "Transmitter Z(m)." An orthogonality is attained using time-division multiplexing (TDM) MIMO wherein each transmitter is activated separately, transmits the signal, and the signal is captured by the receivers. Then, the next transmitter is activated, transmits the signal, and so on. In the MIMO array mode, the beat signal is simulated by the software from the multi-static MIMO array, while in the equivalent phase center (EPC) virtual elements, the beat signal is from the monostatic array containing elements at EPC points of the MIMO array, i.e., virtual elements.

### C. Creating MIMO-SAR Scan Scenario

The four scanning regimes are supported by the software as follows: Linear method requires a collinear antenna array along $y$ dimension and the MIMO array is scanned across the *y*-axis "Y-Step Size" sized steps expressed in wavelength multiples or millimeters using the switch. The rectilinear methods scan the MIMO array across the *x*-*y* plane. The circular scanning method simulates a rotation of the target or axial rotation of the radar around the target to scan the MIMO array across the $\theta$ dimension, it requires the use of a single transceiver pair to synthesize a circular pattern. Lastly, in the cylindrical regime, a cylindrical aperture is synthesized by scanning the MIMO array across the $\theta$ and $y$ dimensions and requires a collinear array. The TDM MIMO SAR mode is used to synthesize the array whereby the signal transmitted by one transmitter is captured by the receivers making up the array at the given step.

### D. Creating the Target Scene

Various methods are available to create the target scenes or import the target, for example, using random points, table of targets, STL (Standard Tessellation Language) and PNG (Portable Network Graphics) file formats etc. The beat signal is computed using either GPU (Graphics Processing Unit) or CPU (Central Processing Unit). The trip path loss can either be included or not. In the table of targets, the reflectivity and exact position of individual point in the scene treated as ideal back scatterers.

### E. Image Reconstruction

The image reconstruction in SAR imaging is a mathematical process that acquires projection data at the target position to generate scene images. The mechanism used for image acquisition and reconstruction process has influence on the image quality [67]. We used the non-uniform C-SAR Back propagation algorithm (BPA) and the uniform C-SAR polar format algorithm (PFA) using the circular and cylindrical scanning methods to acquire 2D and 3D images of the point targets, respectively.

### F. Back Propagation Algorithm Review

The transmitted signal for a SAR imaging system can be expressed as: $s\ (t) = \ Ae^{j2\pi ft}$, where $A$, $j$ and $f$ are the signal amplitude, complex number unit and transmitted signal frequency, respectively. The target's back-scattered wave is: $s\ (m, f) = \delta_m\ s(t)e^{j2\pi f\tau_m}$, where $m$ and $\tau$ are the receiving antenna position and twice signal time delay from the antenna to object, respectively. The time delay $\tau$ is expressed as: $\tau\ =\ 2d/c$, where $c$ is the speed of light and $d$ the distance between target and the antenna. The overall BPA process is defined as:

$$\delta_{BP}\ (x, y, z) = \sum_{m=1}^{M}\sum_{n=1}^{N} s\,(m, f_n)\, e^{-\frac{j4\pi f_n d_m}{c}} \tag{5}$$

where the scanning points are denoted by $M$. From (5), the complex ratio between transmitting and receiving signals can be used to calculate the object function by solving matrix for the given distance. The BPA constructs the object by integrating echoes at distinct frequencies.

### G. Polar Format Algorithm

The polar format algorithm (PFA) is computationally efficient and has been used widely in the spotlight SAR imaging. The PFA process involves firstly applying the reference point matched filter (RMF) and then resampling to the image's wavenumber domain. The consistent processing of the synthetic aperture data by the conventional processes of PFA compromises the efficiency of the PFA algorithm. For the imaging process, azimuth de-chirp is applied to the echo data when using PFA. In range frequency domain, the uniformly matched signal for a bi-static SAR system is:

$$S_d\ (f_\tau, t) = w_a\ \left(\frac{t}{T_a}\right) W_r\ \left(\frac{f_\tau}{B_r}\right) \times e^{-j2\pi\frac{f_c+f_\tau}{c}\Delta R_p(t;x_p,y_p)} \tag{6}$$

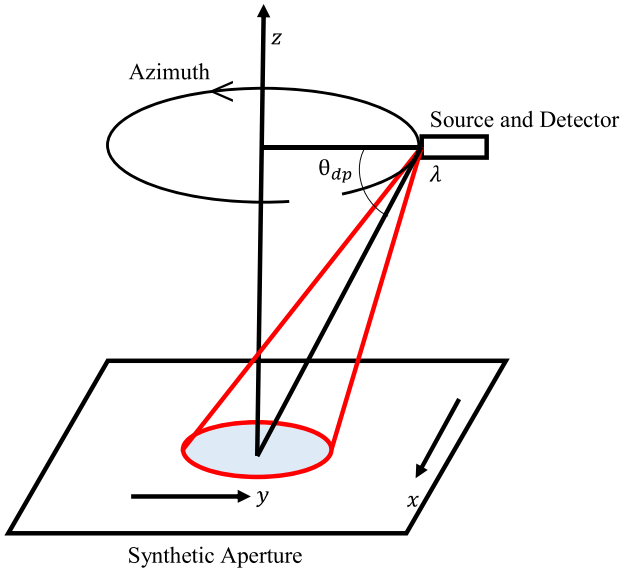


Fig. 3. Circular SAR geometry.

where $w_a$ and $w_r$ are the azimuth and range envelope respectively, $T_a$ is synthetic aperture time, $f_\tau$ is the range frequency variable, $B_r$ denotes the transmitted signal bandwidth and $\Delta R_p$ is the differential range. The full derivation of the PFA image reconstruction process has been derived in [22], [23].

### H. Circular Synthetic Aperture Radar

The curved SAR imaging technology uses curved motion of the radar to acquire omnidirectional 2D or 3D scattering information of the target area. CSAR is a special form of curve SAR and its typical geometry is shown below [2].

For general SAR, the 2D image is acquired through the synthetic aperture in one axis and FMCW for length measurement for the other axis. The spatial resolution in FMCW is determined by the width of the frequency modulation of the source, which is thus limited to several millimeters in THz SAR images. Circular SAR as shown in Fig. 3 scans in a circle and synthetic aperture is applied on both axes, making it possible to obtain 2D image with spatial resolution of several hundred micrometers. When observing an isotropic scatterer at 360°, the resolution can be expressed as:

$$\delta_x = \delta_y\ \sim \frac{\lambda}{4cos\theta_{dp}} \tag{7}$$

### I. Cylindrical SAR

The cylindrical SAR also known as spiral SAR (S-SAR) imaging system is based on cylindrical spiral curve and performs 360° omnidirectional imaging which provides more abundant and comprehensive azimuth scattering information, thereby improving performance for target detection and classification recognition. The typical space trajectory of the S-SAR is shown in Fig. 4.

As shown in Fig. 4, the moving point moves uniformly along the cylindrical busbar and the busbar uniformly rotates the

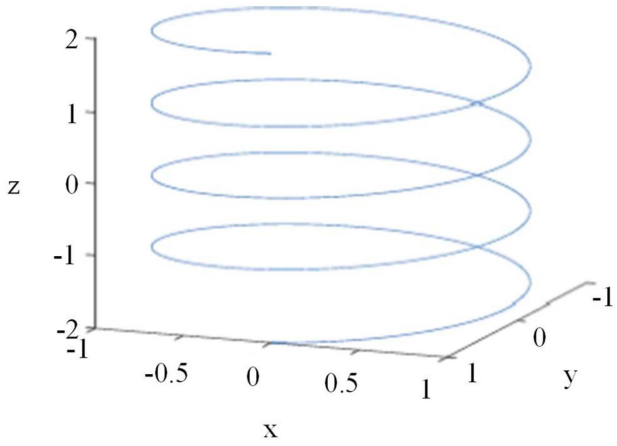


Fig. 4. Cylindrical spiral curve space trajectory [2].

cylindrical surface axis. The moving point composite trajectory motion is called the cylindrical spiral curve which is called right spiral curve when it corresponds to the right-handed rule. The spiral curve is determined by the direction of rotation, Lead (L) or lift angle $\alpha$ and the radius R. The chirp signal transmitted by the radar with bandwidth $B$ and center frequency $f_c$ (assuming energy loss during transmission is negligible) can be expressed as:

$$s\ (\tau, t) = \ rect\left(\frac{\tau}{T_p}\right) \exp\left(j2\pi f_c \tau + j\pi K \tau^2\right) \tag{8}$$

where $rect(.)$ denotes the rectangular window function, $K$ is the chirp rate, $T_p$ is the signal pulse width and $\tau$ is called fast time. The echo signal received by the radar after being reflected by a point target $P$ takes the form:

$$s_r(\tau, t) = \sigma_P \ rect\left[\frac{\tau - \frac{2R_P(t)}{c}}{T_P}\right] \exp\left\{j2\pi f_c \left|\tau - \frac{2R_P\,(t)}{c}\right|\right\} \cdot \exp\left\{j\pi K \left|\tau - \frac{2R_P\,(t)}{c}\right|^2\right\} \tag{9}$$

where $\sigma_P$ is the coefficient of electromagnetic scattering of $P$. After considering reference signal from reference point $O$, adjusting the linear frequency and compensating the video phase term [2], the resultant mathematical model of point target echo signaling SSAR is given by:

$$s_r\ (\tau, t) = \sigma_P \ rect\left[\frac{\tau - \frac{2\Delta R(t)}{c}}{T_P}\right] \exp\left[-j4\pi f \frac{\Delta R\,(t)}{c}\right] \tag{10}$$

where $\Delta R\,(t) = R_P\,(t) - R_O(t)$, $f\ = K_\tau$

## III. Experimental Results and Discussion

The paper focuses on the implementation of the time domain and frequency domain image reconstruction algorithms in THz based FMCW MIMO CSAR which are executed on the CPU of a 64-bit, Intel Core i5, hard disc 1TB personal computer with MATLAB 2020b. A THz and Sub-THz Imaging Toolbox for simulating near-field THz imaging radar systems and image reconstruction developed by the Wireless Information Systems Laboratory (WISLAB) of the University of Texas at Dallas [66], [67] are explored. The toolbox enables rapid development of near field THz imaging radar systems and efficient generation of large near field THz imaging scenarios which are very useful in various data driven applications. Two popular image reconstruction algorithms: BPA and PFA were investigated for point target reconstruction in THz SAR imaging using the novel circular and cylindrical scanning techniques.

TABLE II
Waveform Parameters Parameter

| Parameter | Value (THz) |
|---|---|
| $f_0$ | 3 |
| $f_s$ | 0.0001 |
| $f_c$ | 0.305 |
| $B$ | 0.001 |

### A. Simulation of 2D Imaging

The THz transmit signal in SAR systems can either be continuous or pulse or pulse of Gaussian or chirp etc. [9], here the transmit signal used is the was the chirp signal. The measurements were performed at the FMCW radar chirp parameters, THz center frequency and bandwidth presented in Table II. The THz transmit signal in SAR systems can either be continuous, pulse or pulse of Gaussian or chirp etc. [9], here the transmit signal used is the chirp signal. The measurements are performed at the FMCW radar chirp parameters: starting frequency, sampling frequency, center frequency and bandwidth presented in Table II with $N_k = 50$.

The waveform parameters are set as shown in Table II. The antenna array is set as MIMO antenna array and the scanner configured to simulate the THz imaging-based MIMO-SAR scanning scenario in circular scanning mode instead of the linear, rectilinear, and cylindrical scanning modes. In Fig. 5, the physical array of the Rx and Tx antennas, the synthetic array in the aperture and the MIMO aperture image scenario are displayed. The target scene is created by specifying point targets and computed the beat signal using the CPU. The images from the SAR scenario simulated are reconstructed using the BPA C-SAR and PFA C-SAR reconstruction algorithms to reconstruct 2D radar images.

The results for simulation of two-point targets at the center of scene imaged by a THz-SAR system and reconstructed by the two reconstruction algorithms are shown in Fig. 6. The non-uniform CSAR 2D BPA re-constructor which performs circular scanning and 2D image reconstruction based on the back-propagation algorithm whereby the synthetic aperture spans a circular aperture and two-point targets in the *x-z* plane at the $y = 0$ coordinate is firstly used. Using the same waveform parameters, Rx and Tx antenna arrays, the non-uniform C-SAR 2D PFA re-constructor which performs circular scanning and 2D image reconstruction that is based on the Polar Formatting reconstruction algorithm is used to reconstruct the radar image,

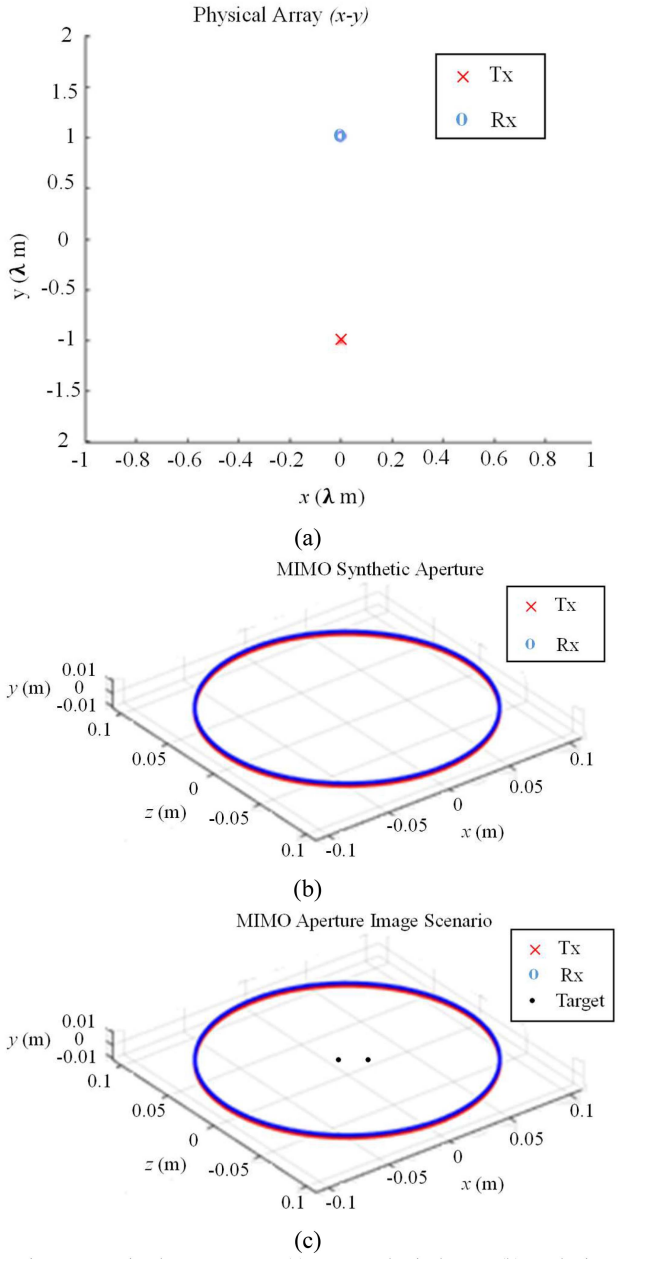


Fig. 5. THz circular SAR set up; (a) antenna physical array, (b) synthetic array, and (c) image scenario.

the synthetic aperture spans the theta dimension to form a circular array and the point target of two points in the $x$-$z$ plane at the $y$-coordinate ($y = 0$).

The target contour in the radar image reconstructed using PFA C-SAR is thinner and clearer. The thin and clearer contour implies an increased ability of target recognition, thus providing basis for subsequent recognition of the target. The ideal images computed for PFA and BPA based reconstruction algorithms are shown in Fig. 7. In the imaging platforms based on SAR, when the chirp pulse signal is sent to the target, the signal reflected from the target contains the information of the target and the chirp. The chirp has to be removed to restore the target.

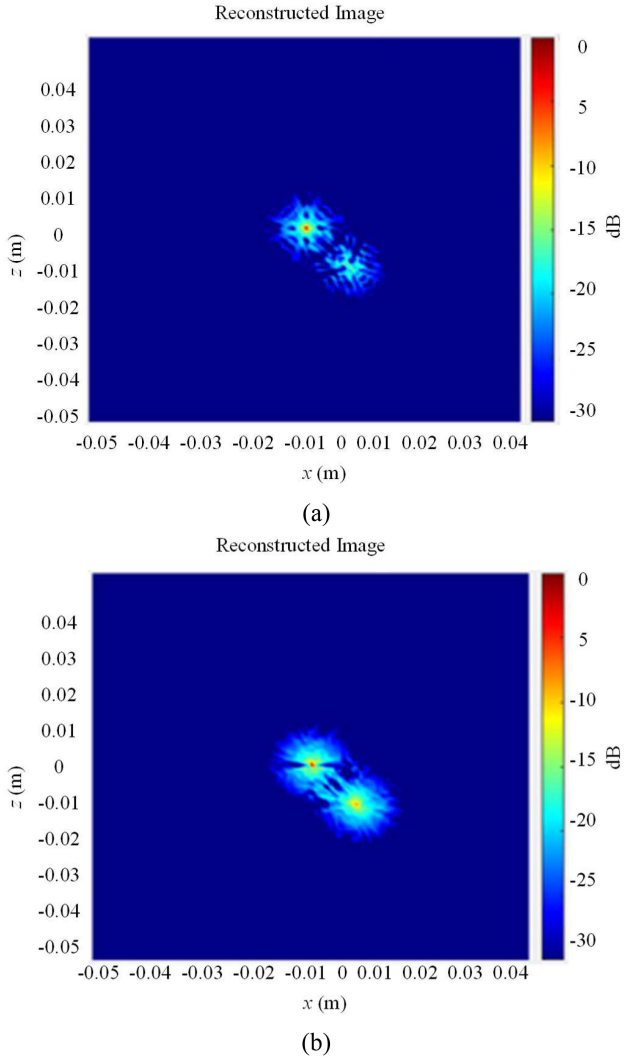


Fig. 6. Reconstructed radar images: (a) C-SAR BPA and (b) C-SAR PFA.

## B. 3D Imaging Simulation

Performing 3D imaging of the target at a stand-off range provides more detail and information for identification or recognition of the target as compared to 2D imaging. Thus, it is useful for instance in tissue imaging applications for offering more anatomical information by enabling measurements from depths of the tissue volume to be examined. There has been an increasing interest in 3D capable THz imaging. In the electro-optic based THz imaging, 3D imaging has been achieved through THz computed tomography which enables non-invasive visualization of the volumetric internal structure and non-destructive, contact free inspection of soft materials [70], [71], [72].

However, the insufficient development status of the conventional THz imaging technology limits the 3D realization due to low spatial resolution. 3D imaging achieved using SAR promises to provide high spatial resolution images that comply with infrared or optical systems. The generation of high resolution 3D SAR image at 1.5THz was demonstrated in [27] using electronic

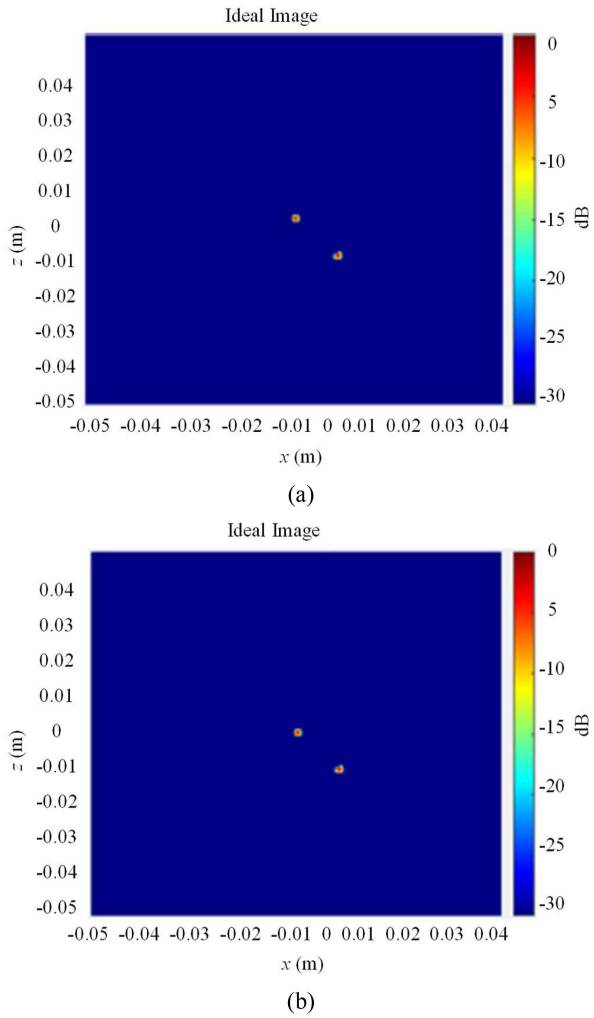


Fig. 7. Computed ideal images (a) BPA ideal image and (b) PFA ideal image.

transceiver modules which can be applied for indoor environmental mapping useful for emergency scenario, rescue missions, object and unconscious human detection and classification etc. To synthesize the aperture along the cross-range direction, the mobile platform with mounted SAR sensors followed a certain trajectory thereby radiating electromagnetic waves towards the target and the backscattered waves recorded. The raw dataset of the recorded signals is then processed with frequency or time domain reconstruction algorithms for reconstructing the image.

The 3D imaging theory could be explained from the representation of the 3D imaging geometry shown in Fig. 8, which extends the 2D imaging where *x*-axis propagation direction provides range information and formation of aperture along the *y*- or *z*-axis acquires the cross-range information to produce an *x*-*y* or *x*-*z* imaging plane such that the *y*- and *z*-axis corresponds to the azimuth direction and elevation direction respectively. For 2D imaging, the 1D trajectory is synthesized in the elevation or azimuth direction and for 3D imaging based on the SAR technique, the 2D trajectory along the elevation and azimuth directions is synthesized to acquire the volumetric information using a planar aperture configuration. Considering the geometry of a monostatic configuration shown in Fig. 8. A transceiver at a

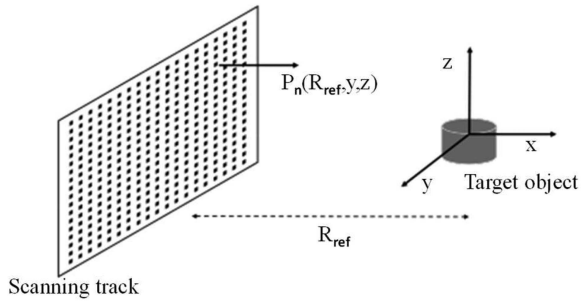


Fig. 8. 3D imaging geometry.

certain point $P_n$ with $n \in (1, N)$ and $N = N_y \times N_z$ being the total positions in the scanning track, $N_y$ and $N_z$ being the number of aperture positions in the azimuth and elevation direction respectively and the $(u, v)$ denoting the coordinates of azimuth and elevation. To model the theory of image reconstruction: consider the transmit signal $p(t)$ in the form of a Gaussian, chirp or single/multi-tone signal. For a transceiver located at $P_n$, the signal received from suppose $L$ scatterers are expressed as:

$$s\ (t, u, v) = \sum_{l=1}^{L} \sigma_l p\left(t - \frac{2R_l}{c}\right) \tag{11}$$

where $\sigma_l$ and $R = \sqrt{(x_l + R_{ref})^2 + (y_l + u)^2 + (z_l + v)^2}$ are the reflectivity from $l$th scatterer and slant range between the transceiver and the $l$th scatter. For the VNA test bed, frequency domain data $S_f$ is firstly gathered and processed with the BPA after zero padding and inverse Fourier transform $s_{t,zp}$. The voxel value at location $(x_i, y_j, z_k)$ in the 3D image reconstructed grid $I$ can be given by:

$$I\ (x_i, y_j, z_k) = \sum_{p=0}^{U} \sum_{m=0}^{V} s_{t,zp}\left(t_{ijk}, u_p, v_m\right) \times \exp\left(-j4\pi f_{\min} R_{ijk}, u_p, \frac{v_m}{c}\right) \tag{12}$$

where $f_{\min}$ is the minimum frequency of zero padded signal and $t_{ijk}$ the roundtrip delay for scatterer at $(x_i, y_j, z_k)$ in $I$. Using the same waveform parameters as presented in Table II, the antenna array is set as MIMO antenna array and the scanner is configured to simulate the THz imaging-based MIMO SAR scanning scenario in cylindrical scanning mode instead of the linear, rectilinear, and circular scanning modes.

In Fig. 9(a) and (b), the physical array of the Rx and Tx antennas, the synthetic array in the aperture and the MIMO aperture image scenario are displayed. The target scene is created by specifying point targets and computed the beat signal using the CPU. The images from the SAR scenario simulated are reconstructed using the uniform CSAR 3D PFA reconstruction algorithm to reconstruct 3D radar images. The results for simulation of two-point targets at the center of scene imaged by a THz SAR system and reconstructed by the reconstruction algorithm are shown in Fig. 9(c). The uniform CSAR 3D PFA re-constructor performs cylindrical scanning and 3D image reconstruction based on the Polar Formatting Algorithm whereby

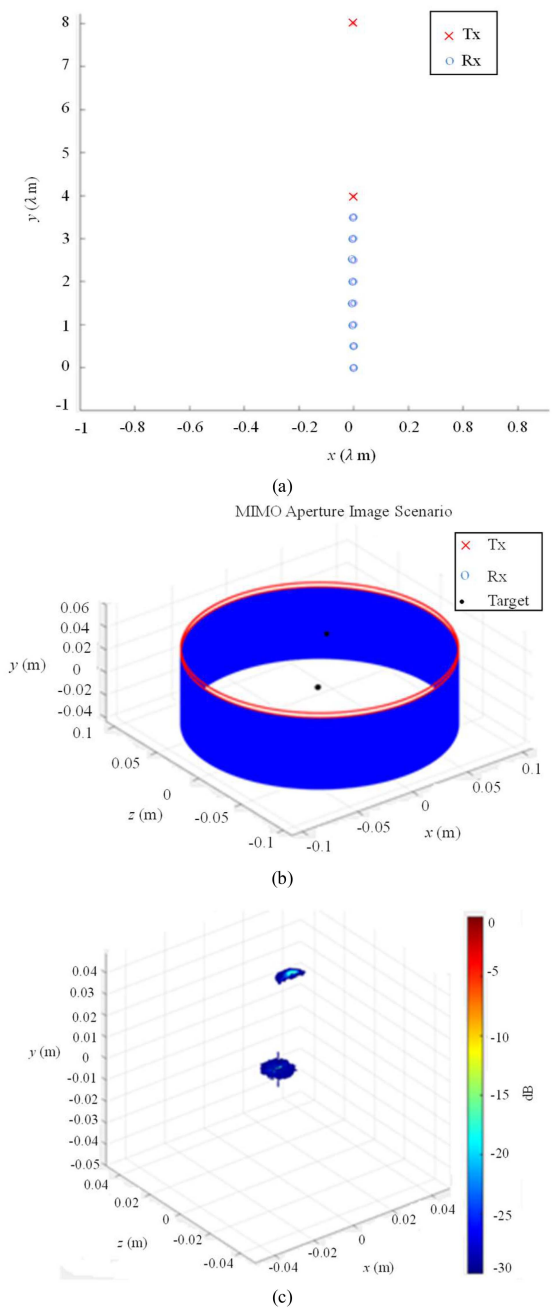


Fig. 9. THz cylindrical SAR imaging set up (a) antenna physical array. (b) MIMO aperture image scenario and (c) 3D radar image.

the synthetic aperture spans across the *y*- and theta dimensions, forming a cylindrical aperture and 2 two-point targets in the *x*-*y*-*z* space are used.

### C. Quality Evaluation Metrics

The measurements of SAR image quality are important to evaluate the performance of a SAR system. The quality evaluation metrics are based on point target analysis. Several metrics are used to evaluate the performance of SAR systems through the formed image quality. Some of the metrics include visual comparisons and automatic metric-based comparisons: spatial resolution, differential resolution, mean square error (MSE), peak signal to noise ratio (PSNR), normalized cross-correlation, average difference, structural content, maximum difference and absolute error. More metrics aligned to radar systems include Peak to Side lobe ratio (PSLR), impulse response (IPR), Additive Noise Levels (ANL), Multiplicative Noise Ratio (MNR), Integrated Side Lobe Ratio (ISLR) and Point Spread Function (PSF) [40]. Visually, the SAR image system distinguished between two target points, indicating good performance. From a visual perspective, the reconstructed images are virtually different in terms of the radar echo enclosing the target as can be seen in Fig. 6. The echo surrounding the BPA C-SAR reconstructed image is blurrier than that of PFA C-SAR which implies more target recognition ability, thus BPA performed better than PFA from the visual perspective.

### D. Algorithms Comparison

Although new image reconstruction algorithms have been proposed continuously, the PFA and BPA algorithms are still being used and suitable for different applications including SAR imaging. In both algorithms, images are formed in space domain: the BPA directly uses the time domain into space domain and in PFA, data is first processed by the reference point matched filtering (RMF) then resampled to wavenumber domain. The resolution features in the two algorithms are different: in BPA, SAR data is focused using accurate Doppler phase in the imaging scene, producing resolution features e.g., side lobe directions and impulse response width that are consistent with range Doppler contour analysis results. For PFA, the image resolution features are dependent on the wavenumber spectrum shape, resulting from far-field planar wave-front assumption being induced and linear spatial variance regularized through polar format mapping [68], [69].

The main advantages of the BPA are its parallelism which makes it ideal for many core devices, for example GPU and hybrid CPU/GPU devices. The BPA is able to focus on any MIMO array configurations resulting in increased design flexibility of MIMO SAR systems. Also, it provides improved performance for locating and focusing objects. However, the BPA suffers high computational burden. The advantages of PFA include that it provides user flexibility with choice for size, resolution and location of the reconstructed image and can project signal history on the focused plane, thereby compensating for non-planar motion of the radar in moving target imaging [73]. Also, PFA is more computationally efficient though it is only accurate in small scene imaging.

### E. Discussion

As presented in the preceding sections, the SAR imaging technology is significantly more established in the Microwave regime of the spectrum as compared to that in the THz whereas THz based SAR brings several potential advantages due to their shorter wavelength, higher carrier frequency, larger bandwidth, higher aperture speed, increased frame rate, which could be exploited for recognition of moving objects and real-time imaging applications. This suggests that most of the currently

available simulators or toolboxes have leveraged Microwave based remote sensing and far-field imaging applications scenarios. Such simulators include: an open-source SAR simulator based on the Shooting and Bouncing Ray (SBR) approach for SAR simulation that uses NVIDIA GPU (Optix GPU), i.e., hardware accelerated computing architectures for unprecedented computational speeds and parallel processing, which is suitable for computationally intensive ray tracing computations. The computational performance of the reported approach has been shown to offer orders of magnitude speed increase over CPU speeds [74]. Another toolbox, free and open-source software has been developed in Python for InSAR simulation for the automatic analysis of artificial radar reflectors. The toolbox is modular and standalone that provides functionality in two layers: analysis of SAR time series without tasks that are computationally demanding and analysis of the full area that includes the analysis of the InSAR time series. The toolbox demonstrates uniqueness in its application and the geodetic community [75]. The S1TBX (Sentinel-1) toolbox which is a part of the SNAP (Sentinel application platform) software has been developed for displaying, reading and writing data from different remote sensing satellites like the ENVISAT, ERS, Sentinel-1. COSMO-SkyMed etc. and is essential for various earth observation applications. Several interferometric and polarimetric tools are included by the toolbox for data generation, preprocessing, registration, calibration, data conversion and speckle filtering etc. [76]. Another InSAR simulator called Delft object-oriented radar interferometric software (DORIS) has been designed by the Delft University's Delft Institute of Earth Observation and Space Systems for generating displacement maps and Digital Elevation Models from Single Look Complex data and for processing satellites data from ENVISAT, RADARSAT, ERS, etc. A MapReady remote sensing toolkit has also been designed that accepts level 1 detected SAR data, optical data from ASF and single look complex SAR data, etc. It is capable of saving various image formats including GeoTIFF [77]. The Broadview Altimetry toolbox has also been designed for reading, recording and computing radar altimetry data from different official data centers such as Envisat, GeoSat and CryoSat, etc. [78], high SAR simulation performance has also been demonstrated by [79] for supporting complex phase dependent processing and analysis based on the SARCASTIC v2.0 engine. Other open source and free toolbox for SAR data processing include but are not limited to the SNAP, Orfeo toolbox, SARbian [80], Xpatch, RaySAR, OptiX SAR [74].

While these simulation tools are versatile and useful for providing the opportunity to mimic radar platform effects under specified environmental conditions, making it possible to theoretically validate the SAR models. There are substantial challenges associated with simulation of real-world data using SAR systems including the subjectivity of the collected SAR signal to noise ratio. On the other hand, the existing THz based SAR imaging studies have mainly focused on several aspects of the performance of reconstruction algorithms as previously reported. Moreover, the THz-SAR is currently very limited with very few open-source implementations.

The THz-SAR simulation is performed as proof of principle and demonstration of the feasibility and validity of SAR based THz imaging for object recognition in indoor environmental monitoring as well as the effectiveness of the explored reconstruction algorithms. The main purpose for exploring the THz-SAR simulation seeks to discover an FMCW THz-SAR for supporting and facilitating data driven research such as deep learning in the THz regime of the spectrum through synthetically generated SAR images. This extends the few currently existing THz-SAR studies previously presented by incorporating synthetic data generation methods. Moreover, the THz-SAR toolbox supports extremely fast GPU parallel processing for unprecedented performance in addition to the advantages provided by THz-SAR that are previously presented. The cumulative impact of this contribution is a SAR simulation tool for near-field imaging, for example, indoor environment monitoring which could be useful for THz based health monitoring.

It can also be shown that the theories and methods explored in this paper have been more broadly explored in the microwave frequency range, with a more recent growing interest to explore SAR in the THz range. However, the application in THz range which has the outstanding capability for breaking diffraction limited spatial resolution has not yet been fully exploited. Based on the findings from literature, the performance of THz based SAR systems is compared to the conventional millimeter wave (mmWave) SAR, where THz-SAR shows potential to outperform microwave SAR due to their higher broadband and frequency spectra as well as capability to operate in harsh weather conditions and provide higher spatial resolution beyond the diffraction limit. Even though the higher frequency spectra suffer limited propagation distance due to higher atmospheric absorption and high path losses, they are suitable for short range applications, for example, indoor environments. Thus, the study shows that THz based SAR systems have the potential for high performance and that new applications are feasible, especially indoor monitoring tasks including for health monitoring. Based on the theoretical analysis, it can be concluded that the THz frequency spectrum provides improved resolution compared to the Microwave spectrum. As an outlook for future publications and improvement of this work, comparative studies will be performed including for comparability of various performance parameters to other simulation works, comparative study on the impact of the different THz frequencies on the quality of the reconstructed image to find the optimum range and comparison of the experimental results with hardware-based results. Further, deep learning models will be developed for extraction of features of the mapped environment for indoor tasks such as detection, classification and localization of the target objects.

## IV. Conclusion and Future Scope

The THz-SAR testbeds are commonly based on FMCW and VNA. In both the algorithms, images are formed in space domain, the BPA directly uses the time domain into space domain and in PFA, data is first processed by the RMF then resampled to wavenumber domain. Here, the PFA is used in reconstructing

both 2D and 3D images because of its robustness and simplicity. This paper seeks to simulate an FMCW MIMO C-SAR geometry for 2D and 3D imaging and explore the potential of THz-SAR system for high resolution imaging in the near-field applications, for example, indoor environments. We have explored the FMCW THz MIMO C-SAR of the THz imaging simulator and the image reconstruction algorithms to circular-and cylindrical/spiral-scanning for near-field THz applications. The THz-SAR image acquisition and C-SAR image reconstruction algorithms are executed to investigate the potential of THz C-SAR based systems. The main intent of the proposed approach is to explore a FMCW THz-SAR to support and facilitate data driven research such as deep learning in the THz community through synthetically generated SAR images. One of the primaries to be addressed in the future is addressing real-time imaging in THz SAR. Due to increased pixels or voxels to be processed in real life applications, the time or computational power requirement for SAR image processing drastically increases in the THz spectrum. The reconstruction algorithms like the BPA inherit a high degree of parallelism and lack data dependencies which can be utilized for computation time reduction. Optimization of architectures for signal processing considering parallel processing can be realized for example, field programmable gate arrays (FPGA), etc. Deep learning-based computing could be developed in THz CSAR imaging applications for improved multimedia experience of users based on distortion correction and efficient, high-speed computing. New network architectures that consider security demands will be required for example, 5G and beyond technologies, also the cyber physical systems for SAR imaging to integrate computing, sensing and communication could be explore through Internet of Multimedia Things (IoMT). The applicability of THz-SAR for health monitoring could be also explored.

## Acknowledgment

The authors are sincerely thankful to the editor and potential reviewers for critical comments and suggestions to improve the quality of the manuscript.

## References

[1] G. Wang, F. Qi, Z. Liu, C. Liu, C. Xing, and W. Ning, "Comparison between back projection algorithm and range migration algorithm in terahertz imaging," *IEEE Access*, vol. 8, pp. 18772–18777, 2020.

[2] C. Lv, B. Deng, Y. Zhang, Q. Yang, and H. Wang, "Terahertz spiral SAR imaging algorithms and simulations," in *Proc. IEEE 4th Inf. Technol., Netw., Electron. Automat. Control Conf.*, 2020, pp. 1746–1750.

[3] A. Batra, M. Wiemeler, D. Göhringer, and T. Kaiser, "Geometrical shapes detection in high-resolution THz SAR image," in *Proc. 19th Eur. Radar Conf.*, 2022, pp. 1–4.

[4] A. Batra et al., "Short-range SAR imaging from GHz to THz waves," *IEEE J. Microw.*, vol. 1, no. 2, pp. 574–585, Apr. 2021.

[5] S. Shi, C. Li, J. Hu, X. Zhang, and G. Fang, "A high frequency vibration compensation approach for terahertz SAR based on sinusoidal frequency modulation Fourier transform," *IEEE Sensors J.*, vol. 21, no. 9, pp. 10796–10803, May 2021.

[6] J. Sun, Z. Hao, Q. Li, and D. Li, "Vibration compensation of airborne terahertz SAR based on along track interferometry," *IEEE Geosci. Remote Sens. Lett.*, vol. 19, pp. 1–5, 2021.

[7] I. Malhotra and G. Singh, "Terahertz near-field imaging and sensing," in *Terahertz Antenna Technology For Imaging and Sensing Applications*. Berlin, Germany: Springer, 2021, pp. 217–234.

[8] N. Wang, T. Chang, and H.-L. Cui, "Nondestructive inspection of packaged microcircuits by aperture-type terahertz near-field imaging," *J. Phys. D: Appl. Phys.*, vol. 55, no. 18, 2022, Art. no. 155105.

[9] A. Batra, M. Wiemeler, D. Goehringer, and T. Kaiser, "Simulation validation of high resolution indoor terahertz synthetic aperture radar imaging," in *Proc. 14th Eur. Conf. Antennas Propag.*, 2020, pp. 1–5.

[10] A. Batra et al., "Object recognition in high-resolution indoor THz SAR mapped environment," *Sensors*, vol. 22, no. 10, 2022, Art. no. 3762.

[11] W. Hu et al., "Ultra-wideband signal generation and fusion algorithm for high-resolution terahertz FMCW radar imaging," *Opt. Exp.*, vol. 30, no. 6, pp. 9814–9822, 2022.

[12] Q. Wang, L. Xie, and Y. Ying, "Overview of imaging methods based on terahertz time-domain spectroscopy," *Appl. Spectrosc. Rev.*, vol. 57, no. 3, pp. 249–264, 2022.

[13] M. Dvorsky, M. T. Al Qaseer, and R. Zoughi, "Synthetic aperture radar 3D polarimetry," *IEEE Trans. Instrum. Meas.*, vol. 71, pp. 1–12, 2022.

[14] V. T. Vu and M. I. Pettersson, "Terahertz three-dimensional SAR imaging using time-and frequency-domain algorithms," in *Proc. IEEE 4th Int. Workshop Mobile Terahertz Syst.*, 2021, pp. 1–5.

[15] S. Saqueb, N. K. Nahar, and K. Sertel, "Fast two-dimensional THz imaging using rail-based synthetic aperture radar (SAR) processing," *Electron. Lett.*, vol. 56, no. 19, pp. 988–990, 2020.

[16] M. Gezimati and G. Singh, "Advances in terahertz technology for cancer detection applications," *Opt. Quantum Electron.*, vol. 55, no. 2, 2023, Art. no. 151.

[17] Z. Li, J. Mei, J. Bai, Y. Xiao, Y. Wang, and J. Zhang, "A terahertz synthetic aperture radar with centimeter-level resolution," in *Proc. IEEE Int. Conf. Infrared, Millimeter, Terahertz Waves*, 2021, pp. 1–2.

[18] Y. K. Chen, Y. C. Lee, and V. C. Koo, "Design and implementation of synthetic aperture radar (SAR) field-programmable gate array (FPGA)-based processor," *Appl. Sci.*, vol. 12, no. 4, 2022, Art. no. 1808.

[19] A. Kamaleldin, E. Aliagha, A. Batra, M. Wiemeler, T. Kaiser, and D. Göhringer, "Hardware/software co-design of 2d THz SAR imaging for FPGA-based systems-on-chip," in *Proc. IEEE 5th Int. Workshop Mobile Terahertz Syst.*, 2022, pp. 1–5.

[20] J. Schorlemer, K. Kolpatzeck, J. C. Balzer, A. Czylwik, I. Rolfes, and J. Barowski, "Efficient frequency domain sampling schemes for THz SAR systems," in *Proc. IEEE 4th Int. Workshop Mobile Terahertz Syst.*, 2021, pp. 1–5.

[21] Y. Luo, D. An, X. Huang, L. Chen, and W. Wang, "A registration strategy for circular SAR noncoherent imaging," in *Proc. IEEE Nat. Radar Conf.*, 2020, pp. 1–4.

[22] L. Fan, Y. Zeng, Q. Yang, H. Wang, and B. Deng, "Fast and high-quality 3D terahertz super-resolution imaging using lightweight SR-CNN," *Remote Sens.*, vol. 13, no. 19, 2021, Art. no. 3800.

[23] S. Hu, C. Shu, Y. Alfadhl, and X. Chen, "Advanced THz MIMO sparse imaging scheme using multipass synthetic aperture focusing and low-rank matrix completion techniques," *IEEE Trans. Microw. Theory Techn.*, vol. 70, no. 1, pp. 659–669, Jan. 2022.

[24] J. W. Smith and M. Torlak, "Efficient 3D near-field MIMO-SAR imaging for irregular scanning geometries," *IEEE Access*, vol. 10, pp. 10283–10294, 2022.

[25] G. Yang et al., "Phase shift migration with modified coherent factor algorithm for MIMO-SAR 3D imaging in THz band," *Remote Sens.*, vol. 13, no. 22, 2021, Art. no. 4701.

[26] Y. Ivanenko, V. T. Vu, J. Barowski, H. Hellsten, and M. I. Pettersson, "Phase control in interpolation for backprojection of THz FMCW SAR signals," in *Proc. IEEE 23rd Int. Radar Symp.*, 2022, pp. 10–15.

[27] A. Batra, M. Wiemeler, D. Gohringer, and T. Kaiser, "Sub-mm resolution 3D SAR imaging at 1.5 THz," in *Proc. IEEE 4th Int. Workshop Mobile Terahertz Syst.*, 2021, pp. 1–5.

[28] A. M. Molaei, S. Hu, V. Fusco, and O. Yurduseven, "A multi-resolution analysis-based approach to accelerate data acquisition for near-field MIMO millimeter-wave imaging," *Proc. SPIE*, vol. 12111, 2022, Art. no. 121110J.

[29] S. Hamidi and S. S. Naeini, "Millimeter-wave circular synthetic aperture radar imaging," in *Proc. IEEE Can. Conf. Elect. Comput. Eng.*, 2021, pp. 1–6.

[30] D. Oloumi, R. S. C. Winter, A. Kordzadeh, P. Boulanger, and K. Rambabu, "Microwave imaging of breast tumor using time-domain UWB circular-SAR technique," *IEEE Trans. Med. Imag.*, vol. 39, no. 4, pp. 934–943, Apr. 2020.

[31] D. Oloumi, P. Boulanger, A. Kordzadeh, and K. Rambabu, "Breast tumor detection using UWB circular-SAR tomographic microwave imaging," in *Proc. 37th Annu. Int. Conf. IEEE Eng. Med. Biol. Soc.*, 2015, pp. 7063–7066.

[32] M. B. Bicer, A. Akdagli, and C. Ozdemir, "A matching-pursuit based approach for detecting and imaging breast cancer tumor," *Prog. Electromagn. Res. M*, vol. 64, pp. 65–76, 2018.

[33] W. Jing, J. Liu, Y. Zhao, G. Jiang, and J. Zhang, "Time-frequency domain hybrid algorithm for near-field MIMO-SAR imaging," *Proc. Int. Conf. Microw. Millimeter Wave Technol.*, 2018, pp. 1–3.

[34] H. Gao et al., "Study of the extended phase shift migration for three-dimensional MIMO-SAR imaging in terahertz band," *IEEE Access*, vol. 8, pp. 24773–24783, 2020.

[35] S. Gishkori et al., "Adaptive subaperture integration for wide-angle synthetic aperture radar," *IEEE Trans. Terahertz Sci. Technol.*, vol. 12, no. 2, pp. 118–129, 2022.

[36] Y. Li, Q. Ji, W. Shi, J. Hong, S. Cheng, and W. Zhang, "Design and simulation of terahertz near field SAR real-time imaging system," *Proc. SPIE*, vol. 11384, 2019, Art. no. 1138413.

[37] X. Kan, M. Cheng, Y. Li, J. Sheng, and C. Fu, "The imaging quality's analysis of terahertz circular SAR affected by the motion error," in *Proc. China Int. SAR Symp.*, 2018, pp. 1–4.

[38] A. Mostajeran, H. Aghasi, S. M. H. Naghavi, and E. Afshari, "Fully integrated solutions for high resolution terahertz imaging (invited)," in *Proc. Custom Integr. Circuits Conf.*, 2019, pp. 1–8.

[39] J. Liu, J. An, R. Zhou, and Y. Yu, "Terahertz near-field MIMO-SAR technology for human security inspection," *Guangdian Gongcheng/Opto-Electron. Eng.*, vol. 47, no. 5, pp. 190681–190682, 2020.

[40] C. Wang, Q. Zhang, J. Hu, C. Li, S. Shi, and G. Fang, "An efficient algorithm based on CSA for THz stepped-frequency SAR imaging," *IEEE Geosci. Remote Sens. Lett.*, vol. 19, 2022, Art. no. 4006505.

[41] C. Sun, J. Wang, R. Zhao, Q. Chang, Y. Wang, and F. Nian, "All-electronic terahertz 3D imaging system based on FMCW," in *Proc. IEEE 46th Int. Conf. Infrared, Millimeter, Terahertz Waves*, 2021, pp. 1–2.

[42] J. P. Guillet, F. Fauquet, A. Chopard, P. Mounaix, J. Rioult, and T. Jaeschke, "Augmented reality terahertz (AR-THz) interface for imaging and sensing," in *Proc. IEEE 46th Int. Conf. Infrared, Millimeter, Terahertz Waves*, 2021, pp. 1–2.

[43] S. Mohammadzadeh et al., "Hand-guided mobile terahertz 3D imaging platform with aspherical telecentric f-$\theta$ optics," in *Proc. IEEE 18th Eur. Radar Conf.*, 2022 pp. 377–380.

[44] J. D. Hawkins, L. B. Lok, P. V. Brennan, and K. W. Nicholls, "Towards a field-ready HF-VHF ground-based ice penetrating synthetic aperture radar: Forward modelling and validation for SAR imaging," in *Proc. IEEE 18th Eur. Radar Conf.*, 2022, pp. 389–392.

[45] O. Csernyava and K. Haneda, "Simulating the radar cross section of a bare tree: From megahertz to terahertz," in *Proc. IEEE 16th Eur. Conf. Antennas Propag.*, 2022, pp. 1–5.

[46] A. Prokscha, F. Sheikh, D. Lessy, N. A. Ali, and T. Kaiser, "Multidisciplinary data fusion for THz ray-tracing," in *Proc. IEEE 16th Eur. Conf. Antennas Propag.*, 2022, pp. 1–5.

[47] R. Kaname, L. Yi, and T. Nagatsuma, "Fast three-dimensional terahertz imaging with continuous-wave photomixing," in *Proc. IEEE 46th Int. Conf. Infrared, Millimeter Terahertz Waves*, 2021, pp. 1–2.

[48] P. Glira et al., "3D mobile mapping of the environment using loading radar sensors," in *Proc. IEEE Radar Conf.*, 2022, pp. 1–7.

[49] N. Kumchaiseemak et al., "Toward ant-sized moving object localization using deep learning in FMCW radar: A pilot study," *IEEE Trans. Geosci. Remote Sens.*, vol. 60, 2022, Art. no. 5112510.

[50] S. Wang, S. Kueppers, H. Cetinkaya, and R. Herschel, "3D localization and vital sign detection of human subjects with a 120 GHz MIMO radar," in *Proc. IEEE 20th Int. Radar Symp.*, 2019, pp. 1–6.

[51] N. Kern, A. Holzbock, T. Grebner, V. Belagiannis, K. Dietmayer, and C. Waldschmidt, "A ground truth system for radar measurements of humans," in *Proc. IEEE 14th German Microw. Conf.*, 2022, pp. 84–87.

[52] N. Sugavanam and E. Ertin, "Models of anisotropic scattering for 3D SAR reconstruction," in *Proc. IEEE Radar Conf.*, 2022, pp. 1–6.

[53] F. Mancuso, E. Giusti, and M. Martorella, "Polarimetric three-dimensional ISAR imaging," in *Proc. IEEE Radar Conf.*, 2022, pp. 1–6.

[54] K. Konishi, K. Ota, M. Tonouchi, and H. Murakami, "Development of a 3D imaging system using millimeter wave MIMO radar," in *Proc. IEEE 46th Int. Conf. Infrared, Millimeter, Terahertz Waves*, 2021, pp. 1–2.

[55] M. M. Tentzeris et al., "Inkjet-/3d -/ 4d -printed nanotechnology-enabled radar, sensing, and RFID modules for internet of things, 'smart skin,' and 'zero power' medical applications," in *Antenna and Sensor Technologies in Modern Medical Applications*. Hoboken, NJ, USA: Wiley, 2021, pp. 399–434.

[56] E. Giusti, S. Ghio, and M. Martorella, "Drone-based 3D interferometric ISAR imaging," in *Proc. IEEE Nat. Radar Conf.*, 2021, pp. 1–6.

[57] B. Gao, F. Zhang, G. Sun, and S. Pan, "High-resolution 3D imaging with a photonics-based broadband MIMO radar," in *Proc. Int. Conf. Microw. Millimeter Wave Technol.*, 2021, pp. 1–3.

[58] M. Maier, F.-N. Stapelfeldt, and V. Issakov, "Design approach of a K-band FMCW radar for breast cancer detection using a full system-level simulation," in *Proc. IEEE MTT-S Int. Microw. Biomed. Conf.*, 2022, pp. 251–253.

[59] S. Wang and R. Herschel, "Fast 3D-CFAR for drone detection with MIMO radars," in *Proc. IEEE 18th Eur. Radar Conf.*, 2022, pp. 209–212.

[60] S. Jardak, D. Yoda, and H. Mori, "Combined ISAR and MIMO processing for near-field 3D radar imaging," in *Proc. 18th Eur. Radar Conf.*, 2022, pp. 409–412.

[61] M. Lotti et al., "Radio simultaneous localization and mapping in the terahertz band," in *Proc. IEEE 25th Int. ITG Workshop Smart Antennas*, 2021, pp. 329–334.

[62] G. Yang, C. Li, S. Wu, X. Liu, and G. Fang, "MIMO-sar 3D imaging based on range wavenumber decomposing," *IEEE Sensors J.*, vol. 21, no. 21, pp. 24309–24317, Nov. 2021.

[63] A. Batra, A. Kamaleldin, L. Y. Zhen, M. Wiemeler, D. Göhringer, and T. Kaiser, "FPGA-based acceleration of THz SAR imaging," in *Proc. IEEE 4th Int. Workshop Mobile Terahertz Syst.*, 2021, pp. 1–5.

[64] L. Yi et al., "Ultra-wideband frequency modulated continuous wave photonic radar system for three-dimensional terahertz synthetic aperture radar imaging," *J. Lightw. Technol.*, vol. 40, no. 20, pp. 6719–6728, Oct. 2022.

[65] H. Li, C. Li, S. Wu, S. Zheng, and G. Fang, "Adaptive 3D imaging for moving targets based on a SIMO InISAR imaging system in 0.2 THz band," *Remote Sens.*, vol. 13, no. 4, 2021, Art. no. 782.

[66] J. Smith and M. Torlak, "Terhertz Imaging Toolbox with interactive user interface," *Wireless Information Systems Laboratory*, 2022, Accessed: Nov. 16, 2022. [Online]. Available: https://labs.utdallas.edu/wislab/projects/

[67] J. W. Smith, M. E. Yanik, and M. Torlak, "Near-field MIMO-ISAR millimeter-wave imaging," in *Proc. IEEE Radar Conf.*, 2020, pp. 1–6.

[68] Y. Miao, J. Wu, J. Yang, and H. Gao, "Comparison between resolution features of BPA and PFA through wavenumber domain analysis for general spotlight SAR," in *Proc. IEEE Int. Geosci. Remote Sens. Symp.*, 2019, pp. 2969–2972.

[69] Y. Song, Y. Hai, J. Wu, Z. Li, and J. Yang, "An efficient PFA subaperture algorithm for video SAR imaging," in *Proc. IEEE Int. Geosci. Remote Sens. Symp.*, 2021, pp. 5179–5182.

[70] Y. C. Hung and S. H. Yang, "Terahertz deep learning computed tomography," in *Proc. IEEE Int. Conf. Infrared, Millimeter, Terahertz Waves*, 2019, pp. 1–2.

[71] R. Ning, D. Wang, L. Rong, Y. Wang, and J. Zhao, "Total-variation iterative algorithm for terahertz transmission computed tomography," in *Proc. IEEE 46th Int. Conf. Infrared, Millimeter Terahertz Waves*, 2021, pp. 1/2.

[72] Y. Jiang, H. Wang, B. Deng, Y. Qin, C. Luo, and Z. Zhuang, "Study of the point spread function of multi-circular synthetic aperture imaging at terahertz frequencies," in *Proc. IEEE 43rd Int. Conf. Infrared, Millimeter, Terahertz Waves*, 2018, pp. 1–2.

[73] Z. Wang, F. Li, X. Peng, and D. Yao, "Circular SAR imaging algorithm based on polar format algorithm for moving target," *J. Eng.*, vol. 2019, no. 19, pp. 5539–5542, 2019.

[74] A. R. Willis, M. S. Hossain, and J. Godwin, "Hardware-accelerated SAR simulation with NVIDIA-RTX technology," *Proc. SPIE*, vol. 11393, 2020, Art. no. 113930O.

[75] R. Czikhardt, H. van der Marel, and J. Papco, "GECORIS: An open-source toolbox for analyzing time series of corner reflectors in InSAR geodesy," *Remote Sens.*, vol. 13, no. 5, 2021, Art. no. 926.

[76] D. Mandal et al., "Sentinel-1 SLC preprocessing workflow for polarimetric applications: A generic practice for generating dual-pol covariance matrix elements in SNAP S-1 toolbox," Preprints.org; 2019, doi: 10.20944/preprints201911.0393.v1.

[77] H. Govil and M. Thakur, "Contribution of L band SAR data for identification of buried/paleochannels in Jaisalmer region of Rajasthan, India," *Adv. Space Res.*, vol. 70, no. 12, pp. 3870–3877, 2022.

[78] A. Mondéjar et al., "Broadview radar altimetry toolbox," *42nd COSPAR Sci. Assem.*, vol. 42, pp. A2–A1, 2018.

[79] M. Woollard, D. Blacknell, H. Griffiths, and M. A. Ritchie, "SARCASTIC v2. 0—High-performance SAR simulation for next-generation ATR systems," *Remote Sens.*, vol. 14, no. 11, 2022, Art. no. 2561.

[80] Z. Chen et al., "Curvilinear flight synthetic aperture radar (CF-SAR): Principles, methods, applications, challenges and trends," *Remote Sens.*, vol. 14, no. 13, 2022, Art. no. 2983.